Proceedings of CONF-MPCS 2026 Symposium: Theoretic Physics and Plasma Physics
DOI: 10.54254/2753-8818/2026.DL35591

Forward Modeling of Galaxy-Scale Strong Gravitational Lensing Images under Multiple Telescope Observing Conditions

Ziqing Li

Department of Physics and Astronomy, University of California, Irvine, USA
ziqinl12@uci.edu

Abstract. Galaxy-scale strong-lensing images are determined not only by the intrinsic lens geometry but also by the observing response, including the point-spread function (PSF), pixel scale, exposure depth, sky noise, stacking blur, and foreground lens light. This paper presents a controlled forward-modeling experiment in which a single intrinsic elliptical power-law lens is held fixed and rendered under Hubble-like, JWST-like, Keck adaptive-optics-like, and survey-like observing conditions. The study uses reproducible image-level diagnostics: arc signal-to-noise ratio, ring completeness, lens-source contrast, compact-feature recovery, and recovery biases in Einstein radius, axis ratio, and mass slope. The survey case adopts a Moffat atmospheric PSF with stacking jitter, and the adaptive-optics case uses a sharp core plus an extended halo. The results show that deep, high-resolution imaging preserves most ring morphology, whereas survey-like imaging retains candidate-level flux but suppresses compact structure and biases the recovered mass slope. The study is not intended to replace full modeling tools such as lenstronomy or PyAutoLens. Its narrower purpose is to isolate how the observing response changes the appearance and interpretation of the same physical lens. The main conclusion is that telescope response is part of the inference model, not a cosmetic correction.

Keywords: strong gravitational lensing, forward modeling, telescope simulation, point-spread function, survey selection

1. Introduction

1.1. Motivation

Strong gravitational lensing occurs when a foreground mass deflects light from a more distant source strongly enough to produce multiple images, arcs, or an Einstein ring. At galaxy scales, these lensed images constrain the projected mass profile of the deflector, the morphology of the background source, the possible presence of dark substructure, and, in some cases, cosmological distances. Strong lensing is a powerful probe because it measures gravitational deflection directly rather than relying solely on emitted light. However, this same strength makes the data

© 2026 The Authors. This is an open access article distributed under the terms of the Creative Commons Attribution License 4.0 (https://creativecommons.org/licenses/by/4.0/).

DOI: 10.54254/2753-8818/2026.DL35591

observationally demanding: much of the relevant scientific information is encoded in detailed image morphology rather than in a single scalar observable [1-4].

A telescope does not record an ideal lens-equation image. Instead, it records an image that has been convolved with the point-spread function (PSF), sampled by detector pixels, contaminated by noise, and blended with foreground lens light. The foreground lens galaxy may be substantially brighter than the lensed source. The PSF spreads compact features over neighboring pixels; the pixel scale determines whether a thin arc is resolved or compressed into a small number of blended samples; and the exposure depth determines whether low-surface-brightness ring segments rise above the background. These effects can transform a visually clean ring into separated arcs, or a genuine lens into an ambiguous survey candidate.

This distinction is important because modern lens modeling is commonly performed at the pixel level. A model that neglects the observing response may reproduce the observed image while still recovering a biased mass slope, biased source size, or spurious residual structure. The risk is greatest when the interpretation depends on faint arcs, compact source clumps, or small residuals that could be attributed to dark substructure. This study therefore treats the telescope and detector response as part of the scientific model. The aim is not to make simulated images visually realistic as a cosmetic exercise, but to determine which physical inferences remain reliable when the same lens is observed under different conditions.

1.2. Research question and contribution

This study addresses a deliberately focused question: for one fixed galaxy-scale strong-lensing system, how do PSF morphology, angular resolution, pixel scale, exposure depth, sky noise, stacking blur, and lens-source brightness contrast affect the detectability and interpretation of arcs and ring structure? The lens mass, source position, source light, and foreground lens light are held fixed, while only the observing response is varied. This design separates the intrinsic lensing geometry from the observational appearance of the system.

The contribution is methodological rather than algorithmic. This paper does not introduce a new public lens-modeling package, a new cosmological inference method, or a complete survey forecast. Instead, it constructs a compact forward-modeling experiment in which the observing response is treated explicitly. The analysis uses four testable components: image-level metrics, a more realistic survey PSF, a compact recovery-bias test, and a comparison with standard modeling software. Together, these components show that passing the same intrinsic lens through different observing models changes the measurable information in quantifiable ways.

The fixed-lens design is also useful for observation planning. Survey images are required to identify rare alignments over large areas, whereas deeper or sharper follow-up observations are needed to interpret the same systems physically. A controlled forward model can identify which observing class is sufficient for candidate discovery, ring tracing, compact-feature recovery, or parameter inference. In this way, image quality becomes a practical decision variable rather than a subjective descriptor.

2. Literature review

2.1. Strong lensing as an image-formation problem

Early galaxy-scale strong-lensing studies showed that arcs and multiple images carry direct information about galaxy mass distributions [1]. Recent reviews emphasize that the observable is

DOI: 10.54254/2753-8818/2026.DL35591

not only the lens mapping, but also the full image after lens light, source light, PSF, detector sampling, and noise have been combined [2, 3]. This point is especially important for dark-matter studies, where small perturbations in arcs may be interpreted as evidence for subhalos or line-of-sight structure [4]. A weak or mismodeled PSF can erase these perturbations or produce misleading residuals.

The current software ecosystem is built around this image-formation view. lenstronomy provides flexible parametric and pixel-based lens modeling with explicit treatment of lens light, source light, PSF convolution, and detector noise [5]. AutoLens and PyAutoLens provide automated modeling workflows, source reconstruction, and Bayesian searches for real and simulated lenses [6, 7]. These tools are broader than the compact pipeline used here. This paper adopts their forward-modeling logic but keeps the parameter space deliberately small, making the controlled comparison easier to interpret.

This distinction is important. A full modeling package is designed to fit data and quantify posterior uncertainty, whereas the compact pipeline in this paper is designed to isolate cause and effect. If a ring segment disappears after the PSF is broadened, the change can be attributed to the observing model because the intrinsic lens has not been altered. This design does not replace package-level modeling; rather, it provides a diagnostic layer before physical claims are drawn from a complex fit.

2.2. Survey discovery and follow-up context

Strong-lens discovery is shifting from small hand-selected samples to survey-scale searches. The strong-lens finding challenge showed that classification performance depends on resolution, depth, contrast, and contamination by non-lens objects [8]. A recent review of lens searches emphasizes the same difficulty across galaxies, quasars, supernovae, fast radio bursts, gamma-ray bursts, and gravitational waves: a lens is scientifically useful only after it can be recognized against many false positives [9]. Survey-scale statistical models also show that detectability must be treated as a selection function, not as a fixed property of the source-lens geometry [10].

These issues are especially important for Rubin, Euclid, JWST, and upcoming radio surveys. Rubin is expected to transform the time-domain and wide-area strong-lensing sample [11]. Euclid early-release work has already demonstrated the role of machine learning and visual inspection in finding lenses in high-resolution survey images [12, 13]. JWST lens searches in COSMOS-Web and other deep fields show how depth and near-infrared sensitivity reveal high-redshift lenses and faint arcs that may be weak or absent in shallower data [14]. Radio forecasts add a complementary warning: when Einstein radii approach the PSF scale, discovery strategies must account for blending and multi-survey information [15].

Recent reconstruction methods and time-domain applications reinforce the same point. LensCharm and related Bayesian approaches emphasize uncertainty propagation in image reconstruction [16]. Lensed supernova and time-delay cosmography studies require careful measurements of fluxes, delays, microlensing, and line-of-sight effects in addition to the lens geometry [17, 18]. New subhalo-detection forecasts show that the detectability of dark substructure depends strongly on the observation properties and on the assumed lens model [19]. Recent JWST blank-field searches further show that even visually clean arcs require consistent photometry and foreground modeling before they become reliable science targets [20].

DOI: 10.54254/2753-8818/2026.DL35591

3. Methodology

3.1. Fixed physical lens

The simulation uses a single intrinsic lens system throughout the experiment. The deflector mass follows an elliptical power-law profile with Einstein radius θ_E = 1.0 arcsec, logarithmic slope γ = 2.0, projected axis ratio q = 0.76, and position angle 28°. The foreground lens light and background source light are modeled with Sersic profiles. Two compact Gaussian source clumps are included to test whether small-scale structure survives the observing process. All image coordinates are given in arcsec, and all detector values are reported in counts.

The lensing geometry follows the standard mapping between the image-plane angular coordinate θ and the source-plane coordinate β:

$$\beta = \theta - \alpha(\theta) \tag{1}$$

Here, $\alpha(\theta)$ is the scaled deflection field. Lens light is evaluated in the image plane, whereas source light is evaluated at β; therefore, the background source is lensed before the telescope response is applied.

The resulting clean sky image is then passed through the detector model:

$$D_{ij} = S_{ij}\{[I_L(\theta) + I_S(\beta)] * P\} + N_{ij} \tag{2}$$

In Eq. (2), D_{ij} is the detector image, I_L is the foreground lens light, I_S is the ray-traced source light, P is the PSF, S_{ij} denotes pixel sampling, and N_{ij} is the noise realization. The photometric scale is

$$m = -2.5log_{10}(F) + ZP \tag{3}$$

and the total noise variance is approximated as

$$\sigma_{ij}^2 = D_{ij} + B_{ij} + RN^2 \tag{4}$$

where B_{ij} is the sky or detector background, and RN is the read noise. This expression emphasizes the central point: detectability is controlled by signal-to-noise ratio, not by lens geometry alone.

3.2. Observing response models

The observing classes are representative rather than exact engineering replicas. They isolate the effects most relevant to the interpretation of lens images: angular resolution, PSF morphology, pixel scale, exposure depth, and sky noise. The Hubble-like case provides a stable high-resolution benchmark. The JWST-like case tests deep near-infrared follow-up. The Keck adaptive-optics-like case tests a sharp core with an extended atmospheric halo. The survey-like case tests wide-field candidate discovery with coarse pixels, seeing, and stacking blur.

The survey PSF is not treated as a pure Gaussian. Instead, it is modeled as a Moffat profile with β = 3 and an additional 0.18 arcsec stacking-jitter term. Although simplified, this approximation is closer to ground-based survey imaging because atmospheric wings and coadd registration errors spread arc light more strongly than a narrow Gaussian. The adaptive-optics model uses a two-component core-plus-halo PSF to mimic residual atmospheric structure. These additions directly

DOI: 10.54254/2753-8818/2026.DL35591

address the concern that a Gaussian PSF can overstate arc sharpness. The pixel scales, PSF assumptions, FWHM values, exposure times, and intended stress tests for each observing class are summarized in Table 1.

Table 1. Representative observing inputs used in the forward-modeling comparison

Class	Pixel(arcsec/ pix)	PSF model	FWHM (arcsec)	Exposure (s)	Key stress
Hubble-like	0.050	Gaussian	0.090	900	Stable high-resolution imaging
JWST-like	0.031	Gaussian	0.070	3000	Deep faint-arc recovery
Keck AO-like	0.025	Core + halo AO PSF	0.055 core; 0.20 halo	1200	Sharp core with atmospheric residuals
Survey-like	0.200	Moffat $\beta = 3$ +0.18 arcsec jitter	0.750	600	Seeing, stacking blur, and coarse sampling

3.3. Quantitative diagnostics

To avoid subjective descriptions such as visible arcs or continuous rings, the analysis defines explicit diagnostics. The arc mask is based on the noiseless lensed source in the 0.45-1.55 arcsec annulus. Ring completeness is measured in 36 angular bins from 0.55 to 1.45 arcsec. A bin is counted as detected when the source signal-to-noise ratio exceeds 3 and the source-to-lens ratio exceeds 0.5. Ring completeness is defined as

$$C_{ring} = N_{det} \ / \ 36 \tag{5}$$

where N_{det} is the number of detected angular bins. This metric is not intended to provide a full reconstruction score. Instead, it measures whether enough of the ring remains above the noise and foreground light to support modeling. The full set of image-level diagnostics, their definitions, and their physical interpretations are summarized in Table 2.

Table 2. Image-level metrics used in the analysis

Diagnostic	Definition	Interpretation
Arc S/N	ΣS_{arc} / sqrt($\Sigma\sigma^2$)	Total detectability of the lensed source
Ring completeness C_{ring}	Fraction of 36 angular bins with $S/\sigma > 3$ and $S/L > 0.5$	How much of the ring remains usable
Lens-source index	Median S/L over the arc mask	Foreground-blending severity
Compact recovery R_{comp}	max(source after PSF) / max(source before PSF)	Survival of clumps and small features
Recovery bias	Refit θ_E, q, and γ after convolution	Bias in key lens parameters

3.4. Recovery experiment and software comparison

To connect image appearance with physical inference, a compact recovery test is included. After each observing model is applied, the mock image is refit for θ_E, q, γ, and source flux. The recovery fit deliberately assumes a single Gaussian PSF. This approximation is nearly adequate for the space-like cases but mismatched for the adaptive-optics and survey cases. The mismatch is intentional: it tests how strongly simplified observing assumptions can bias the recovered parameters.

DOI: 10.54254/2753-8818/2026.DL35591

The comparison with standard software is therefore framed cautiously. The pipeline used here is not a replacement for lenstronomy, AutoLens, or PyAutoLens. Those packages support broader mass models, pixelized sources, Bayesian search strategies, and real-data workflows [5-7]. The present pipeline is shorter and less general. Its advantage is control: the same intrinsic lens is rendered under several observing assumptions, and the change in diagnostic score can be traced directly to the observing response. The role of the compact pipeline relative to common strong-lensing software packages is summarized in Table 3.

Table 3. Position of the compact model relative to common strong-lensing software

Package or model	Strength	Role in this paper
This compact pipeline	Short controlled fixed-lens experiment	Computes the diagnostics and bias table
lenstronomy	Flexible analytic lens/light models and forward fitting	Reference convention for elliptical power-law ray tracing
PyAutoLens / AutoLens	Automated modeling, source reconstruction, Bayesian workflows	Benchmark context for future full refits

4. Results and discussion

4.1. Visual feature survival

The fixed lens changes appearance substantially when only the observing response is changed. Figure 1 shows detector-level images with foreground lens light included. The Hubble-like and JWST-like cases preserve a recognizable ring, although the arc still overlaps with the central lens galaxy. The Keck adaptive-optics-like case retains high angular detail but also shows a noisier halo structure. The survey-like case preserves a broad candidate-level flux excess but suppresses thin ring morphology.

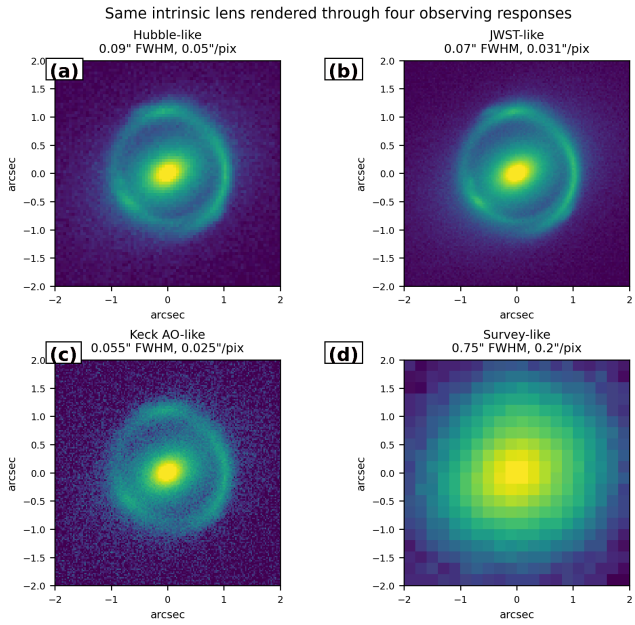

Figure 1. Same intrinsic lens rendered through four observing responses: (a) Hubble-like, (b) JWST-like, (c) Keck AO-like, and (d) survey-like. Axes are in arcsec

DOI: 10.54254/2753-8818/2026.DL35591

Figure 2 shows lens-light-subtracted residuals, which correspond more directly to the images used for the quantitative diagnostics. The space-like residuals retain curvature and azimuthal variation. The adaptive-optics residual preserves sharp substructure, but the background is rougher because the PSF halo and noise are harder to model. The survey-like residual retains arc flux, but the pixels are too coarse to recover compact clumps reliably. The same physical lens therefore supports different levels of inference under different observing responses.

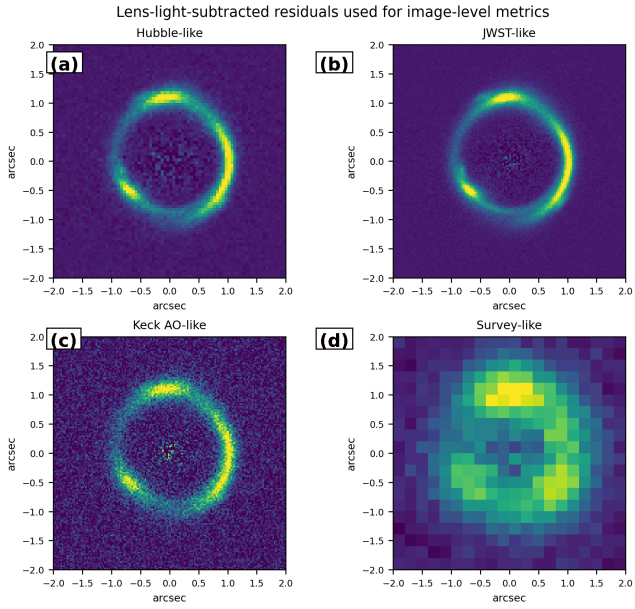

Figure 2. Lens-light-subtracted residuals used for image-level metrics: (a) Hubble-like, (b) JWST-like, (c) Keck AO-like, and (d) survey-like

The main visual result is that image quality changes the scientific question. In high-resolution data, it is reasonable to analyze ring curvature, source clumps, and local residuals. In survey-like data, candidate recognition is the safer goal. Treating these images as equivalent would overstate the survey case and understate the need for follow-up.

4.2. Quantitative metric results

The metrics make the visual differences more precise. Table 4 shows that the space-like cases reach full ring completeness in this controlled setup. JWST-like imaging has the highest arc signal-to-noise ratio because of its deeper exposure. The Hubble-like case has a lower signal-to-noise ratio but still preserves the full ring. The Keck adaptive-optics-like case retains substantial compact information, but the structured PSF and noise reduce ring completeness. The survey-like case contains enough total signal for candidate identification, yet its lens-source index and compact-feature recovery are much weaker.

Table 4. Quantitative results; biases come from the simplified recovery fit

Class	Arc S/N	C_{ring} (%)	S/L	R_{comp}	$\Delta\theta_E$ (%)	Δq (%)	$\Delta\gamma$ (%)
Hubble-like	276.8	100	1.71	0.68	-0.04	-0.09	-0.03
JWST-like	594.5	100	1.82	0.75	-0.02	0.04	-0.04
Keck AO-like	182.9	75	1.48	0.52	-0.39	4.37	-5.97

DOI: 10.54254/2753-8818/2026.DL35591

Table 4. (continued)

Survey-like	114.6	64	0.44	0.13	0.70	5.14	-9.72

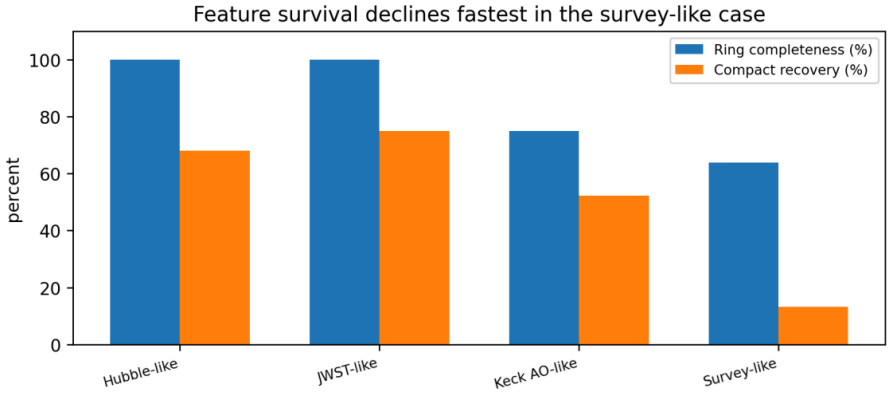

Figure 3. Ring completeness and compact-feature recovery from Table 4

Figure 3 highlights the main contrast: ring completeness declines moderately, whereas compact-feature recovery collapses in the survey-like case. This behavior is expected. Broad seeing spreads clump flux over many pixels, and coarse sampling reduces peak contrast. The clumps are not physically absent; they are observationally diluted. A model that attempts to infer source structure from the survey-like image alone would therefore be underconstrained.

4.3. Recovery biases and interpretation

The recovery test connects image morphology to lens parameters. In this controlled experiment, the Hubble-like and JWST-like cases recover θ_E, q, and γ with sub-percent bias. This does not imply that space-based imaging is free of systematics. Rather, it indicates that, for this simple mock system, the Gaussian recovery PSF is sufficiently close to the true PSF for the main lens parameters to remain stable. The result changes when the PSF mismatch becomes stronger.

The Keck adaptive-optics-like image preserves fine structure, but the simplified Gaussian recovery underfits the PSF halo. The recovered mass slope γ is biased by -5.97%. The survey-like image has the weakest source-lens separation, the lowest compact recovery, and the largest slope bias, -9.72%. These biases are not caused by a change in the physical lens; they arise from the observing model and the simplified recovery assumption. This is the central result of the paper.

This result should not be interpreted as a telescope ranking. Survey-like imaging is essential because it covers enough sky to find rare alignments. Adaptive optics is valuable because it can resolve compact structures when the PSF is well calibrated. JWST-like imaging is powerful for faint red sources and low-surface-brightness arcs. Hubble-like imaging remains a stable high-resolution benchmark. Each observing class has a distinct role, and the forward model identifies which claims are appropriate for each role.

The most robust interpretation is comparative. Features that persist after changes in PSF, pixel scale, exposure depth, and lens-source contrast are more reliable. Features that appear only under one observing response require follow-up or a full package-level refit before they are used to support physical claims. A missing counterimage in a survey image is weak evidence for physical absence. Similarly, a sharp adaptive-optics residual is weak evidence for substructure until the PSF halo, lens-light subtraction, and source model have been tested.

DOI: 10.54254/2753-8818/2026.DL35591

4.4. Practical implications for observing strategy

A practical observing plan should match data quality to the scientific task. A survey-like image can flag a candidate for later inspection, but it is not sufficient for measuring a mass slope, identifying compact source clumps, or testing dark substructure. For those tasks, the forward model points toward deeper imaging, a sharper PSF, or both.

This logic also helps prioritize follow-up. A candidate with high total arc signal but low compact recovery should be treated as promising but incomplete; high-resolution follow-up may recover the lost structure through better sampling. A candidate with low ring completeness and strong foreground contamination may require color separation and lens-light modeling before additional exposure time is useful.

The metrics are intentionally simple enough to be reused. A future survey team could compute arc S/N, ring completeness, foreground contrast, and compact recovery for simulated candidates before running full Bayesian fits. Such diagnostics would not replace detailed modeling, but they would accelerate the first decision: which candidates are ready for quantitative inference, and which require better data first.

5. Limitations and future work

This study remains a compact controlled experiment. It uses one lens, one source, simplified throughput values, and representative observing classes. It includes a Moffat survey PSF and stacking jitter, but it does not include field-dependent PSFs, chromatic aberration, spatially varying sky background, detector persistence, cosmic rays, correlated noise from real image reduction, or full multi-band lens-light subtraction. The numerical values should therefore be interpreted as demonstration-level results rather than final performance forecasts for specific facilities.

The recovery test is also deliberately limited. It refits only a small set of parameters and uses a simplified PSF. A real analysis should fit the mock images with lenstronomy and PyAutoLens, allow a broader family of mass models, include both pixelized and parametric source reconstructions, and propagate posterior uncertainty. A useful next step is a mock catalog spanning many source morphologies, lens ellipticities, flux ratios, and redshifts. The diagnostic table could then be converted into completeness and bias curves for discovery, confirmation, and precision modeling.

Multi-band modeling is another important extension. Color can help separate lens and source light, but chromatic PSFs and band-dependent morphology can also introduce bias. Future simulations should include realistic sky backgrounds, field-dependent PSFs, dithering patterns, and lens-finding algorithms. Those tests would connect the controlled results here to survey operations. The main conclusion would remain the same, but it would rest on a stronger statistical foundation.

6. Conclusion

This paper presents a forward-modeling study of galaxy-scale strong gravitational lensing images under multiple observing conditions. The intrinsic lens is fixed, while PSF morphology, angular resolution, pixel scale, exposure depth, sky noise, stacking blur, and lens-source contrast are varied. This controlled design isolates observation-driven changes from changes in the physical lens system.

The result is clear: the same lens can appear as a clean ring, a noisy arc system, or a blended survey candidate. These differences are measurable. Arc signal-to-noise ratio, ring completeness, lens-source contrast, compact-feature recovery, and recovery bias all vary with observing response. Space-like cases preserve the ring well. Adaptive-optics-like data preserve compact detail but

DOI: 10.54254/2753-8818/2026.DL35591

require careful PSF treatment. Survey-like data are effective for discovery but risky for detailed slope or source-structure inference without stronger modeling.

The central scientific message is direct: telescope response is part of the science. It should be modeled before residuals, missing arcs, compact clumps, or parameter shifts are interpreted as physical. Forward modeling is therefore more than a visualization tool. It provides a guardrail for observation planning and reliable strong-lensing inference.

Declaration of interest

The author declares that there are no known competing financial interests or personal relationships that could have appeared to influence the work reported in this paper.

Authorship

Ziqing Li: conceptualization, methodology, simulation design, visualization, analysis, writing - original draft, and writing - review and editing.

References

[1] Treu, T. (2010). Strong lensing by galaxies. *Annual Review of Astronomy and Astrophysics, 48*, 87–125. https://doi.org/10.1146/annurev-astro-081309-130924

[2] Shajib, A. J., Vernardos, G., Collett, T. E., Motta, V., Sluse, D., Williams, L. L. R., Saha, P., Birrer, S., Spiniello, C., & Treu, T. (2024). Strong lensing by galaxies. *Space Science Reviews, 220*, 87. https://doi.org/10.1007/s11214-024-01105-x

[3] Saha, P., Sluse, D., Wagner, J., & Williams, L. L. R. (2024). Essentials of strong gravitational lensing. *Space Science Reviews, 220*, 12. https://doi.org/10.1007/s11214-024-01041-w

[4] Vegetti, S., Birrer, S., Despali, G., Fassnacht, C. D., Gilman, D., Hezaveh, Y., et al. (2024). Strong gravitational lensing as a probe of dark matter. *Space Science Reviews, 220*, 58. https://doi.org/10.1007/s11214-024-01087-w

[5] Birrer, S., & Amara, A. (2018). lenstronomy: Multi-purpose gravitational lens modelling software package. *Physics of the Dark Universe, 22*, 189–201. https://doi.org/10.1016/j.dark.2018.11.002

[6] Nightingale, J. W., Dye, S., & Massey, R. J. (2018). Autolens: Automated modeling of a strong lens's light, mass, and source. *Monthly Notices of the Royal Astronomical Society, 478*, 4738–4784. https://doi.org/10.1093/mnras/sty1264

[7] Nightingale, J. W., Hayes, R. G., Kelly, A., Amvrosiadis, A., Etherington, A., He, Q., et al. (2021). Pyautolens: Open-source strong gravitational lensing. *Journal of Open Source Software, 6*(58), 2825. https://doi.org/10.21105/joss.02825

[8] Metcalf, R. B., Meneghetti, M., Avestruz, C., Bellagamba, F., Bom, C. R., Bertin, E., et al. (2019). The strong gravitational lens finding challenge. *Astronomy & Astrophysics, 625*, A119. https://doi.org/10.1051/0004-6361/201832797

[9] Lemon, C., Courbin, F., More, A., McMahon, R. G., et al. (2024). Searching for strong gravitational lenses. *Space Science Reviews, 220*, 23. https://doi.org/10.1007/s11214-024-01042-9

[10] Ferrami, G., & Wyithe, J. S. B. (2024). A model for galaxy-galaxy strong lensing statistics in surveys. *Monthly Notices of the Royal Astronomical Society, 532*, 1832–1848. https://doi.org/10.1093/mnras/stae1607

[11] Shajib, A. J., Smith, G. P., Birrer, S., Verma, A., Arendse, N., Collett, T., Daylan, T., & Serjeant, S. (2025). Strong gravitational lenses from the Vera C. Rubin Observatory. *Philosophical Transactions of the Royal Society A, 383*(2295), 20240117. https://doi.org/10.1098/rsta.2024.0117

[12] Pearce-Casey, R., Nagam, B. C., Wilde, J., Busillo, V., Ulivi, L., Andika, I. T., et al. (2025). Euclid: Searches for strong gravitational lenses using convolutional neural nets in Early Release Observations of the Perseus field. *Astronomy & Astrophysics, 696*, A214. https://doi.org/10.1051/0004-6361/202453152

[13] Lines, N. E. P., Li, T., Collett, T. E., Holloway, P., Nightingale, J. W., Rojas, K., Verma, A., & Walmsley, M. (2025). The revolution in strong lensing discoveries from Euclid. *Nature Astronomy, 9*(8), 1116-1122. https://doi.org/10.1038/s41550-025-02616-5

DOI: 10.54254/2753-8818/2026.DL35591

[14] Nightingale, J. W., Mahler, G., McCleary, J., He, Q., Hogg, N. B., Amvrosiadis, A., et al. (2025). The COSMOS-Web Lens Survey (COWLS) I: Discovery of more than 100 high-redshift strong lenses in contiguous JWST imaging. *Monthly Notices of the Royal Astronomical Society, 543*, 203-222. https://doi.org/10.1093/mnras/staf1253

[15] McCarty, S., & Connor, L. (2025). Strong gravitational lensing with upcoming wide-field radio surveys. *Monthly Notices of the Royal Astronomical Society, 542*, 2494-2509. https://doi.org/10.1093/mnras/staf1381

[16] Ruestig, J., Guardiani, M., Roth, J., Frank, P., & Ensslin, T. A. (2024). Introducing LensCharm: A charming Bayesian strong lensing reconstruction framework. *Astronomy & Astrophysics, 682*, A146. https://doi.org/10.1051/0004-6361/202348256

[17] Suyu, S. H., Goobar, A., Collett, T., More, A., & Vernardos, G. (2024). Strong gravitational lensing and microlensing of supernovae. *Space Science Reviews, 220*, 13. https://doi.org/10.1007/s11214-024-01044-7

[18] Birrer, S., Millon, M., Sluse, D., Shajib, A. J., Courbin, F., Erickson, S., Koopmans, L. V. E., Suyu, S. H., & Treu, T. (2024). Time-delay cosmography: Measuring the Hubble constant and other cosmological parameters with strong gravitational lensing. *Space Science Reviews, 220*, 48. https://doi.org/10.1007/s11214-024-01079-w

[19] Kollmann, K. E., Nightingale, J. W., Lisanti, M., Robertson, A., & Slone, O. (2026). Using strong lensing to detect subhaloes with steep inner density profiles. *Monthly Notices of the Royal Astronomical Society, 546*(4), stag066. https://doi.org/10.1093/mnras/stag066

[20] Ferrami, G., Adams, N. J., Westcott, L., Harvey, T., Jansen, R. A., Diego, J. M., et al. (2026). Galaxy-scale lens search in the PEARLS NEP TDF and CEERS JWST fields. *Monthly Notices of the Royal Astronomical Society, 545*(2), staf1991. https://doi.org/10.1093/mnras/staf1991